CONF-950401--25
SAND 94-2825C

A COMPARISON OF PRESSURE COMPACTION AND DIAMETRAL COMPRESSION TESTS FOR DETERMINING GRANULE STRENGTHS

S. Jill Glass and Clay Newton, Sandia National Labs, Albuquerque, NM, 87185

ABSTRACT

Pressure compaction (P-C) tests were used to characterize the strength of ceramic granules. When compaction data are plotted as relative density of the compact versus the compaction pressure two linear regions are generally observed. The intersection of these regions, which is known as the "breakpoint," has been used as a semi-quantitative measure of granule strength. Comparisons were made between the P-C breakpoint and strengths of 150-200 μm diameter ZnO, TiO_2 (rutile), and lead magnesium niobate - lead titanate (PMN-PT) granules, where the strengths were determined by diametral compression (D-C) tests. At high compaction pressures the compliance of the die itself is significant and was accounted for in the analyses. Tests were conducted at different compaction rates, and with different aspect ratio compacts. High aspect ratios and loading rates decrease the slope of the second linear portion of the compaction curve and produce higher apparent P-C breakpoints. Comparison of the P-C breakpoint to the average D-C strength indicates that the D-C strength is approximately fifty percent higher for PMN-PT granules. To eliminate the uncertainty in the results due to irregular granules sizes and shapes, comparisons were also made for uniform size (210 μm) glass spheres. In this case the average D-C strength coincided with a second breakpoint in the P-C data, which occurred after compaction by a mechanism of bridge formation and collapse had ceased.

INTRODUCTION

Lightning strikes can cause structural damage, ignite flammable materials, and produce circuit malfunctions in missiles, aircraft, and ground systems. Lightning arrestor connectors (LACs) are used to divert harmful lightning energy away from these systems by providing less destructive breakdown paths. Ceramic granules in the size range of 150-200 μm are used in LACs to provide physical and electrical separation of contacts (pins) from the surrounding metal web, and to control the voltage breakdown level. ZnO varistor materials, TiO_2, and lead magnesium niobate - lead titanate (PMN-PT) have been used as the granule material. LACs can

be subjected to vibrational stresses that may exceed the granules' fracture strength and lead to a degradation in LAC performance; therefore granule strength is a critical material parameter. The two tests selected to determine granule fracture strength were a pressure compaction (P-C) test,[1-3] and a diametral compression (D-C) test for individual granules.[4-6] The objectives of the study were to determine how to obtain reproducible results from pressure compaction tests, and to determine the relationship between the P-C breakpoint and the D-C strength. Tests were conducted on ZnO, rutile, and PMN-PT granules. For the PMN-PT granules, tests were conducted on materials fired at temperatures between 800 and 1200°C to correlate granule strength with processing history.

LITERATURE REVIEW

Compaction Testing

Pressure compaction tests have been widely used to characterize the strength of powders, agglomerates, granules, and aggregates.[2,3] The compaction test can be used as a quality control tool to determine if powders and granules display acceptable compaction behavior for subsequent forming by dry pressing or isostatic pressing. Bruch was one of the first to use compaction curves to interpret ceramic consolidation behavior.[7] The compaction process depends on the deformation properties of the powders or granules, compaction parameters such as loading rate, die design, and the dimensions and shape of the compacted body. Much effort has been devoted to defining general compaction equations, studying density and pressure distributions in dies,[8] and characterizing the compaction behavior of particulate materials.[9] Mahoney and Readey review compaction models in another paper in this volume.[10]

Compaction Mechanisms

Compaction of ceramic granules occurs in three general stages: 1) granule rearrangement and sliding without fracture; 2) local deformation and fracture of granules; and 3) sliding and rearrangement of particles or fracture fragments within granules.[11] Although the compaction mechanisms have been described as distinct stages, there are components of each during the entire compaction process.[12] When load-deflection data from a compaction test are plotted as relative density vs. log compaction pressure, the data often exhibit distinct linear regimes as shown schematically in Fig. 1. Walker (1923) first observed this behavior for both metallic and non-metallic powders.[13] In many compaction models, including that of Reed and Runk,[1] regions 1) and 2) are distinguished from each other by a parameter known as the breakpoint. Before the breakpoint there is very little density increase with pressure as the granules undergo rearrangement without fracture. The second linear region represents granule rearrangement in conjunction with granule fracture. The breakpoint is a semi-quantitative indicator of the fracture stress of the granule, and the different linear regions of the compaction diagram are thought to represent the pressure regimes where different compaction mechanisms predominate.

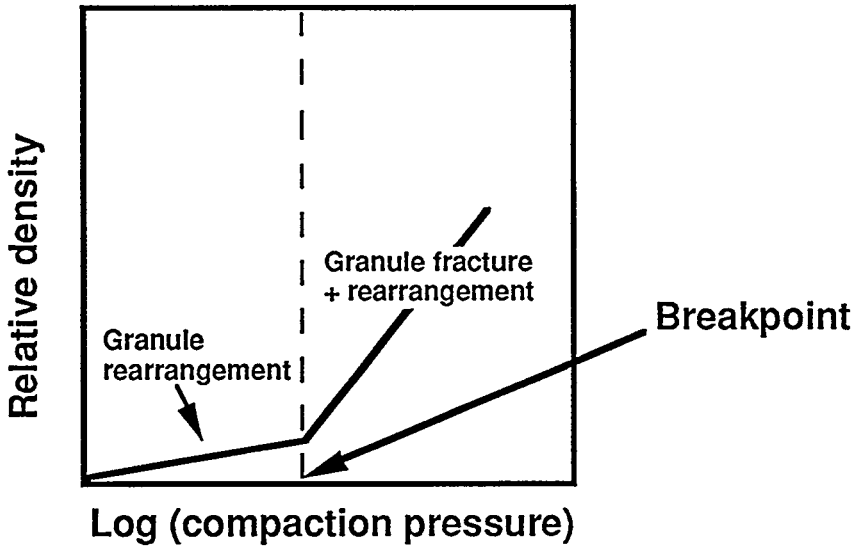

Fig. 1. Semilogarithmic compaction curve exhibiting characteristic linear regions separated by the breakpoint.

Experiments

To obtain meaningful data from compaction tests, they must be conducted under standardized conditions and experimental errors due to contributions from the deformation of the testing equipment must be minimized. Data from tests where these experimental errors have not been accounted for or minimized often exhibit nonsensical behavior on compaction plots, making it impossible to identify material characteristics and compaction mechanisms. Matsumoto pointed out that errors can occur due to contributions from the load-frame, die, compact, and load cell, but in his tests the only significant contribution was from the load cell.[14] Baconegra showed that die compliance can also be significant.[15] Experimental approaches for minimizing such errors have been described by Mort et al.[16]

Diametral Compression Strength Measurements

Granule and agglomerate strengths have also been measured in diametral compression tests, where single granules are loaded in compression between platens until fracture occurs. The granule tensile strength, σ_t, is calculated from the fracture load, P_{max}, and the granule diameter, d, using Hiramatsu's and Oka's equation:[6]

$$\sigma_t = \frac{2.9\ P_{max}}{\pi d^2} \qquad (1)$$

Equation 1 has been used in numerous studies.[4,17,18]

EXPERIMENTAL PROCEDURE

Pressure Compaction (P-C) Tests

A cylindrical die with a 3.2 mm diameter opening was used for pressure compaction tests. Tests were conducted at ambient temperature and humidity with no die lubrication. Unlike typical spray-dried ceramic granules, all of the granules in this study had been fired to sufficiently high temperatures to remove all organic materials. All had also undergone some degree of densification during firing. Three or more samples were tested from each batch of granules. Nominally 0.06 g of PMN-PT granules were compacted to final aspect ratios, L_f/D, of 0.36 to 0.42 (where L_f=final compact height and D=compact diameter). For the rutile tests three masses were used that corresponded to final aspect ratios of L_f/D=0.69 for 0.06 g, L_f/D=1.18 for 0.10 g, and L_f/D=2.58 for 0.20 g. The die was filled using a funnel or creased weighing paper, and no attempt was made to increase the tap density by shaking or vibrating the die.

P-C tests were conducted by loading the filled die in a mechanical testing load-frame. The crosshead was moved incrementally to make contact with the top plunger of the die until a positive load of approximately one to two pounds was indicated. The displacement gauge was then zeroed and the crosshead was activated at a rate of 0.127 mm/min. The test was continued until a compressive load of approximately 422 MPa (60 ksi) was reached. Tests on rutile granules were also conducted at a rate of 0.635 mm/min. Load cell and displacement gauge indications were collected one to two times per second for the P-C tests.

Errors due to the deformation of the loadframe and load cell were eliminated by measuring the displacement of the top plunger relative to the die body. To account for the error due to the deformation of the top plunger of the fixture, the displacement of the empty fixture as a function of load was subtracted from the displacement of the granule-filled die. Displacement data were converted to relative densities using granule mass, initial compact height, measured displacement (corrected for empty die displacement), and theoretical density. Relative density and compaction pressure were plotted as relative density vs. log of the compaction pressure. When displayed in this manner, the data exhibit the expected linear regions. Best-fit lines were drawn through the data in the two linear regions and the pressure at the intersection of the best-fit lines was recorded as the breakpoint.

Diametral Compression Tests

To measure granule strength individual granules were compressed between platens on a mechanical testing load-frame. The granule diameter, d (assumed to be the height of the granule as it was positioned between the platens), was measured using a microscope, camera, and video monitor. The granule was fractured by lowering the upper platen at 0.0508 mm/min or 0.127 mm/min. Twenty or more granules of each material were fractured. Granule tensile strength was calculated using Eq. 1.

RESULTS AND DISCUSSION

Pressure Compaction Results

Figure 2 shows a typical plot of how compact relative density changes with increasing compaction pressure for ZnO granules. As expected, two linear regions, corresponding to Stages 1 and 2 in powder compaction are observed. The results also show that die plunger displacement can contribute to additional deformation at high compaction pressures, which can lead to erroneous interpretation of the data. For example, the uncorrected data indicate an erroneously high relative density. At the highest compaction loads the die plunger deformation accounts for approximately 9% of the total measured displacement of the plunger for a filled die. The uncorrected data also incorrectly indicate a lower apparent breakpoint, and more granule fracture and rearrangement after the breakpoint. Thus the correction for die plunger deformation is necessary in order to make valid measurements of how changes in the granule properties themselves affect the compaction behavior and parameters such as the breakpoint.

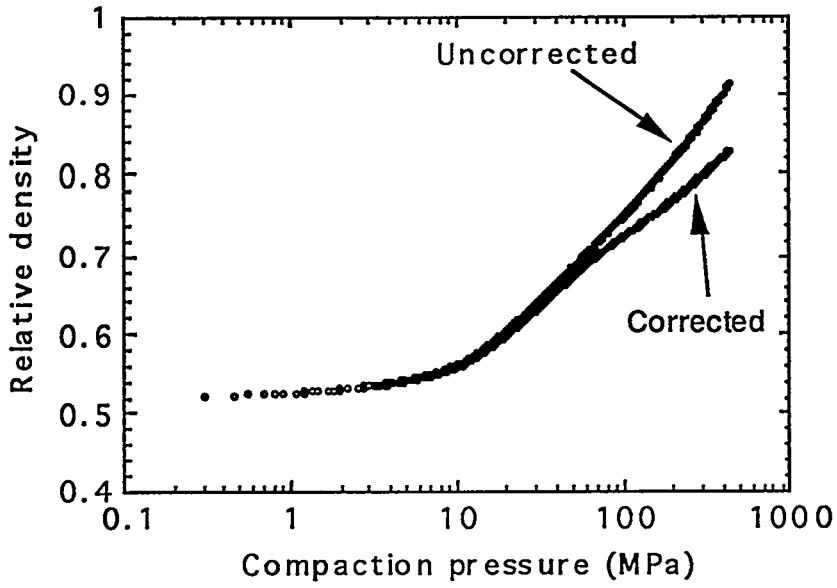

Fig. 2. A typical compaction curve for ZnO granules. Comparison of uncorrected data to data that accounts for deformation of the fixture shows that die plunger deformation at high pressures represents ~9% of the total displacement. This error produces erroneously high densities and a lower apparent breakpoint.

The effect of aspect ratio on compaction behavior for rutile granules is shown in Fig. 3. Tests conducted at $L_f/D = 0.7$ and 1.2 gave similar results; however, $L_f/D = 2.6$ gave a lower final density, a smaller slope in the second linear region of the

compaction curve, and a higher apparent breakpoint. Die wall friction effects, which lead to stress gradients in powder and granular compacts, and which are known to be more extreme in higher aspect ratio compacts,[19] are the source of this effect. The decreased slope is a clear indication that a significant number of the granules are being subjected to stresses less than the applied stress. In the presence of significant stress gradients, higher applied pressures must be exerted before many of the granules in the compact are subjected to their failure stress. Because both of the lower L_f/D values produced similar curves, it appears that these values are below the limit necessary to ensure uniform stress transmission in the compact for these types of material.

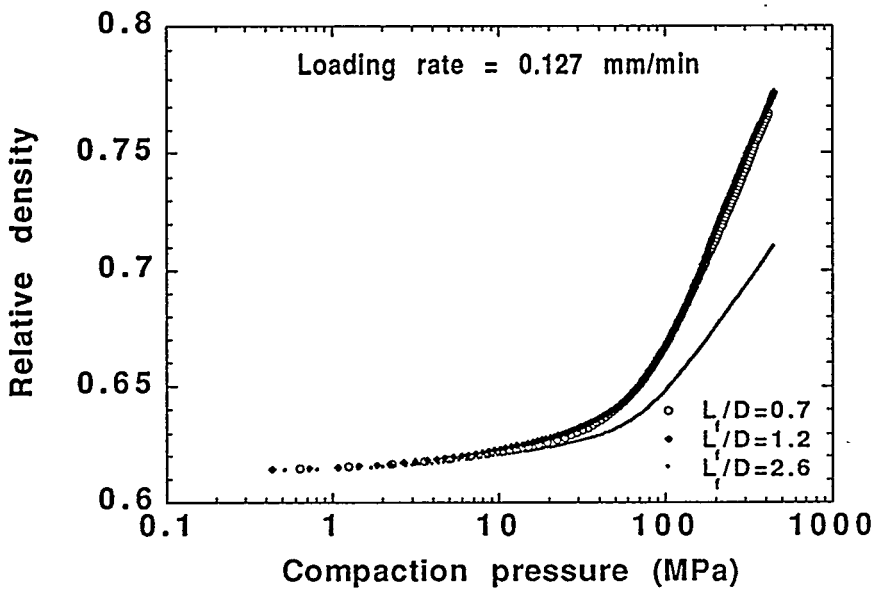

Fig. 3. Effect of aspect ratio, L_f/D on the compaction behavior of rutile granules. For $L_f/D \leq 1.2$ similar compaction curves are obtained. At $L_f/D = 2.6$ the final density is lower, and the slope of the second linear region is smaller, producing a higher apparent breakpoint.

The effect of loading rate on the compaction behavior of rutile granules is shown in Fig. 4. Although the loading rates used in this study are very slow relative to those used in commercial pressing operations, there is a noticeable effect of the higher loading rate. The increased loading rate decreases the slope of the second linear region of the compaction curve, increases the apparent breakpoint, and produces a lower final density. The effect is likely due to the fact that the higher loading rate provides less time for sliding and rearrangement of granule fragments following fracture. Two previous studies showed that higher loading rates (0.508 to 5.08 mm/min,[9] and 0.25 and 5.0 mm/min,[2]) retard the onset of compaction by granule

fracture and rearrangement, but produced a higher slope once this compaction mechanism began. The higher slope is opposite to the effect that was observed in the present study; however, in both of these studies the loading rate effect was associated with viscous deformation of powder-binder systems. The granules in the present study contain no binder.

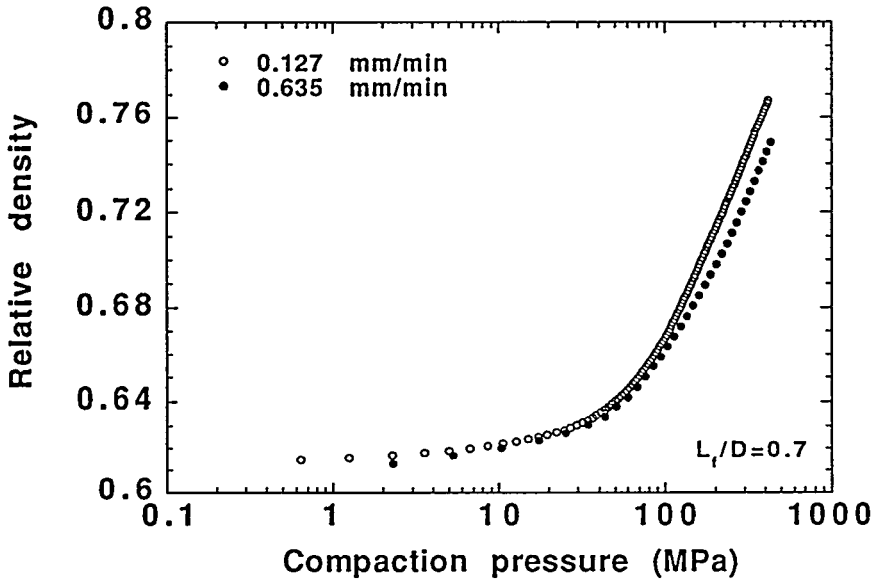

Fig. 4. Effect of loading rate on the compaction behavior of fired rutile granules. The higher loading rate results in a lower final density and the slope of the second linear region is smaller, resulting in a higher apparent breakpoint.

Compaction tests on PMN-PT granules fired at temperatures between 800 and 1200°C were conducted at the slower loading rate of 0.127 mm/min, with masses that produced aspect ratios less than $L_f/D = 0.5$. The objective of this part of the study was to identify the firing temperature that produced granules with the highest strength for use in the lightning arrestor connector application. The compaction behavior as a function of firing temperature is shown in Fig. 5. As the firing temperature increases the initial density increases, the breakpoint initially increases and then decreases, and the final density generally increases. The breakpoint increase between 800 and 1000°C, which is interpreted as an increase in granule strength, is likely related to increased granule density. At temperatures greater than 1000°C further density increases are limited; however, grain growth within the granules becomes significant leading to a decline in the breakpoints and strength.

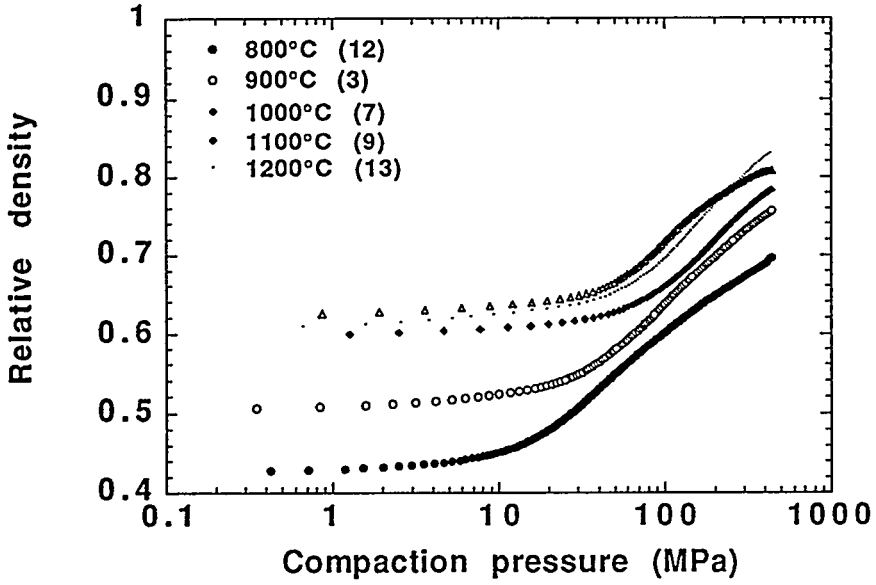

Fig. 5. Compaction behavior of lead magnesium niobate - lead titanate (PMN-PT) granules as a function of firing temperature. Initial density increases as firing temperature increases and breakpoint increases to a maximum at 1000°C.

Compaction results are shown in Fig. 6 for the uniform size 210 μm glass spheres. The final aspect ratio, Lf/D, was 0.68. This compaction data exhibits three linear regions with two breakpoints, the first at 86 MPa (12.4 ksi) and the second at 171 MPa (24.9 ksi). Examination of the data between the two breakpoints reveals that jumps in density are accompanied by significant load drops, consistent with major rearrangements. One compaction test was terminated at approximately 138 MPa (20 ksi). The presence of broken glass spheres indicated that the density increases are due to a combination of sphere fracture and rearrangement, and not just due to major rearrangements.

Diametral Compression Results

The average D-C strength data for some of the PMN-PT granules are shown in Fig. 7 along with the P-C breakpoints for the same materials. The D-C strengths are on average ~50% higher than the breakpoints. Similar results were obtained for rutile granules and PMN-PT granules of different compositions. These results are in contrast to those of Song and Evans who found that the D-C strength of 20-40 μm spray-dried ZrO_2 agglomerates was ~52% of the breakpoint.[18] Although we have not used the approach of Song and Evans, whereby the area fraction of

agglomerates that transmits the force through the assembly is accounted for, this correction would lower our breakpoint values and move them farther from our D-C strengths. The reason the results of this study are in contrast to those of Song and Evans is presently unknown; however, it seems logical that the breakpoint should be lower than the average D-C strength because the breakpoint is the stress near the onset of granule fracture. Hence a better comparison would be made between the P-C breakpoint and the lowest D-C strengths, rather than the average D-C strength.

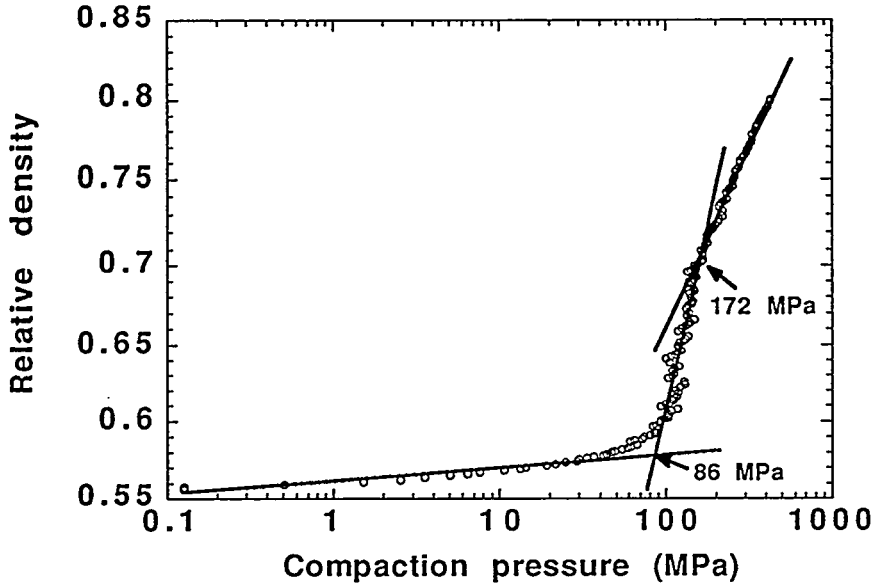

Fig. 6. Compaction behavior of uniform 210 μm diameter glass spheres. Three linear regions and two breakpoints are observed.

The D-C strength data for PMN-PT granules are shown in Table I along with the breakpoints from Fig. 6. Due to the inherent brittle nature of ceramics, the range of granule sizes, and the irregular shape of the PMN-PT granules (with the consequent difficulty in determining a granule diameter), there is considerable scatter in the D-C data; however, the lowest values in the D-C strength distribution correspond more closely to the breakpoints than the average D-C strengths do.

To eliminate the uncertainty associated with the irregularity of the PMN-PT granules, D-C strengths were also measured for uniform size (210 μm) glass spheres and compared to their P-C breakpoint. The glass spheres also have a uniform spherical shape, which minimizes stress concentrations that can lead to lower apparent strengths for irregularly shaped granules. The glass sphere D-C strength data are also shown in Table I.

Table I. Diametral compression strength data for PMN-PT granules and uniform size glass spheres.

Material	Avg. Strength (MPa)	Range (MPa) Min-Max	Breakpoint (MPa)
PMN-PT, 900°C	47 ± 16	23 - 80	24
PMN-PT, 1000°C	94 ± 35	32 - 181	56
PMN-PT, 1100°C	60 ± 19	16 - 102	50
PMN-PT, 1200°C	46 ± 16	13 - 79	34
			1st 2nd
Glass (210 μm)	379 ± 166	127 - 584	86 172

The glass sphere average D-C strength of 379 MPa (55 ksi) greatly exceeds both breakpoint strengths; however, it appears that the lowest D-C strengths in the distribution correspond most closely to the second P-C breakpoint of 172 MPa (24.9 ksi). Because spheres are breaking at compaction stresses between the first and second breakpoints, at stresses less than the lowest strength spheres, some appear to sustain stresses much higher than the applied stress.

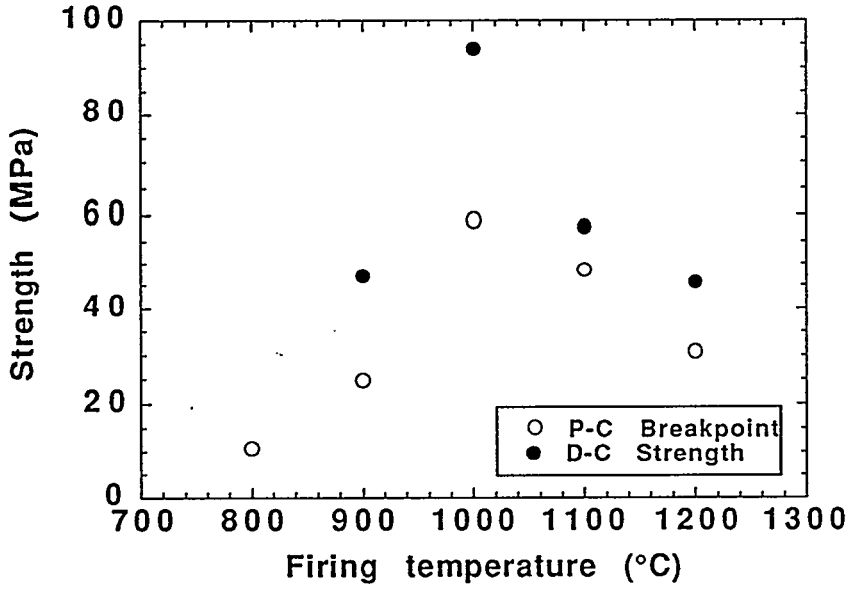

Fig. 7. Diametral compression (D-C) strength and pressure compaction (P-C) breakpoint as a function of firing temperature for lead magnesium niobate - lead titanate (PMN-PT) granules.

A possible mechanism for this is the formation of load-bearing bridges or chains. This mechanism has also been observed by discrete element modeling (DEM).[20] The bridge mechanism also explains the P-C results in Fig. 6. When a sphere in a load-bearing bridge fractures, significant rearrangement of the sphere assemblage occurs. The load is also no longer supported by a bridge and it decreases until another bridge forms. This is consistent with the density increases and accompanying load drops observed in the second linear region of the compaction curve in Fig. 6.

At stresses of ~ 172 MPa (25 ksi), the mechanism of bridge formation and collapse appears to end, and compaction of spheres under a more uniform applied stress begins. The stresses at the onset of this compaction mechanism are close to the low range of the D-C strength distribution. Thus in compaction tests where bridge formation and collapse occurs, the compaction stress that corresponds most closely to the granule strength is the second breakpoint.

The compaction mechanism of bridge formation and collapse was not observed in tests on ZnO, rutile, or PMN-PT granules. This may be due to the fact that these granules exhibit a range of sizes, and fill space in such a way that bridges do not form. The irregular shape of these granules and the possibility that small pieces of the granule break off under pressure, rather than the entire granule fracturing in half or shattering may also play a role in their tendency not to form bridges. Fracture of small regions of the granule would not allow the major rearrangements that are typical following the fracture of a glass sphere. Absence of bridge formation and collapse may also be related to the fact that significant rearrangement cannot occur following granule fracture, due to the roughness of the surface of the polycrystalline granules and their irregular shape. Granules appear to become locked in place at much lower pressures.

CONCLUSIONS

To identify compaction mechanisms, to make valid comparisons between one material and another, and to obtain reproducible results, experimental errors must be accounted for, and compaction test conditions must be standardized. In this study the error due to die deformation was 9% at the highest loads (420 MPa) and results in a higher density and a lower apparent breakpoint. Final aspect ratios, $L_f/D \leq 1.2$ produce consistent compaction results for rutile granules. $L_f/D=2.6$ values decreased the final compaction density, and decreased the slope of the second linear region of the curve. This effect is due to stress gradients in compacts with high aspect ratios. Increased loading rates affect the compaction curve in the same manner as high aspect ratios. This effect is due to the fact that granules have less time to rearrange at higher loading rates. The average D-C strengths of PMN-PT granules are approximately 1.5 times higher than the P-C breakpoints; however, the low range of the D-C strength distribution is close to the breakpoint stress. This is consistent with the breakpoint representing the stress near onset of granule fracture, and not the average granule strength. Glass sphere compaction data exhibited two breakpoints; the first represents the stress at the onset of compaction due to bridge

formation and collapse, and the second represents the onset of compaction due to granule fracture and rearrangement under a more uniform applied stress. Bridge formation and collapse does not appear to play a significant role in compaction of ZnO, rutile, or PMN-PT granules.

ACKNOWLEDGMENTS
This work was supported by the U.S. Dept. of Energy under contract No. DE-AC04-94AL85000 at Sandia National Laboratories.

REFERENCES

1. J. S. Reed and R. B. Runk, "Dry Pressing," pp. 71 in Treatise on Materials Science and Technology, Vol. 9, Ceramic Fabrication Processes, Edited by F. F. Y. Wang, Academic Press, NY, 1976.
2. G. L. Messing, C. J. Markhoff, and L. G. McCoy, "Characterization of Ceramic Powder Compaction," J. Am. Ceram. Soc., 61 [8] 857 (1982).
3. B. J. McEntire, "Dry Pressing," pp. 141-146 in Vol. 4, Engineered Materials Handbook, Ceramics and Glasses, ASM International, 1991.
4. J. Y. Wong, S. E. Laurich-McIntyre, A. K. Khaund, and R. C. Bradt, "Strengths of Green and Fired Spherical Aluminosilicate Aggregates," J. Am. Ceram. Soc., 70 [10] 785-91 (1993).
5. P. T. Bertrand, S. E. Laurich-McIntyre, and R. C. Bradt, "Strengths of Fused and Tabular Alumina Refractory Grains," Am. Ceram. Soc. Bull., 67 [7] 1217-22 (1988).
6. Y. Hiramatsu and Y. Oka, "Determination of the Tensile Strength of Rock by a Compression Test of an Irregular Test Piece," Int. J. Rock Mech. Min. Sci., Vol. 3, pp. 89-99 (1966).
7. C. A. Bruch, "Problems in Die-Pressing Submicron Size Alumina Powder," Ceram. Age, 83 [10] 44-53 (1967).
8. R. A. Thompson, "Mechanics of Powder Pressing I-III," Am. Ceramic. Soc., Bull., 60 [2] pp. 237-245 (1981).
9. R. A. Youshaw and J. W. Halloran, "Compaction of Spray-Dried Powders," J. Am. Ceram. Soc., 61 [2] 227-230 (1982).
10. F. M. Mahoney and M. J. Readey, "Ceramic Compaction Models: Useful Design Tools or Simple Trend Indicators?," Proceedings of the Symposium on "Science, Technology and Commercialization of Powder Synthesis and Shape Forming Processes," Apr. 30-May 4, 1995, ACerS Annual Meeting, Cincinnati, Ohio.
11. R. A. DiMilia and J. S. Reed, "Dependence of Compaction on the Glass Transition Temperature of the Binder Phase," Am. Ceram. Soc. Bull., 62 [4] 484-488 (1983).
12. A. R. Cooper, Jr. and L. E. Eaton, "Compaction Behavior of Several Ceramic Powders," J. Am. Ceram. Soc, 45 [3] pp. 97-101 (1962).
13. C. L. Huffine and C. F. Bonilla, "Particle-Size Effects in the Compression of Powders," AIChE J., 8 [4] 490-93 (1962).
14. R. L. K. Matsumoto, "Generation of Powder Compaction Response Diagrams," J. Am. Ceram. Soc., 69 [10] C246-247 (1986).

15. M. H. Bocanegra, "The Break Point in the Pressure-Density Curve of Magnesia Prepared by the Sea Water Magnesia Process," J. Mater. Sci., 28 (1993), 3467-3472.
16. P. R. Mort, R. Sabia, D. E. Niesz, and R. E. Riman, "Automated Generation and Analysis of Powder Compaction Diagrams," Powder Tech., 79, pp. 111-119, (1994).
17. H. Kamiya, K. Isomura, and G. Jimbo, and T. Jun-ichiro, "Powder Processing for the Fabrication of Si_3N_4 Ceramics: I, Influence of Spray-Dried Granule Strength on Pore Size Distribution in Green Compacts," J. Am. Ceram. Soc., 78 [1] 49-57 (1995).
18. J-H. Song and J. R. G. Evans, "A Die Pressing Test for the Estimation of Agglomerate Strength," J. Am. Ceram. Soc., 77 [3] 806-14 (1994).
19. A. W. Janssen, "Versuche uber Getreiderdruck in Silozellen (Experiments on Grain Pressure in Silos)," Z. Ver. Dtsch. Ing., 39, 1045-49 (1895).
20. G. G. W. Mustoe, G. L. DePoorter, and D. R. Greening, "Methodology for Discrete Numerical Modeling of Powder Compaction Processes," Proc. of the First Inter. Conf. on Adv. Synthesis of Engineered Materials, San Francisco, CA, 31 Aug. - 2 Sept., 1992, pp. 73-79, ASM International.

DISCLAIMER